Scenario Based Ground Motion Simulations for Istanbul, Turkey

E. Zengin & E. Cakti
Bogazici University, Istanbul, Turkey

SUMMARY:
We perform a stochastic finite fault simulation in the Istanbul area (Turkey), based on several fault rupture scenarios. The Istanbul area is divided into approximately 12,000 grids of size 800mx800m, and synthetic site-specific ground motions are generated for each grid, using fault rupture scenarios, systematically-calibrated model parameters, and detailed site investigation studies. The region-specific source, path, and site model parameters are calibrated by simulating the M_l5.1 Marmara Sea Earthquake, which occurred on July 25, 2011 on the Central Marmara Fault Segment. The calibrated model parameters are used to generate grid-based site-specific synthetics in the city of Istanbul for a M7.4 earthquake. The effect of hypocenter location, stress drop and pulsing percentage changes on ground motion is studied. The simulation model parameters are verified by comparing the simulation results and ground motion prediction equations.

Keywords: simulation, ground motion, stochastic, scenario-based, Istanbul

1. INTRODUCTION

Earthquake risk in the city of Istanbul has become a matter of significant concern after the 1999 Kocaeli (Mw=7.4) and Duzce (Mw=7.2) earthquakes, which occurred along the North Anatolian Fault (NAF). Because these large earthquakes caused an increase in the Coulomb stress along the Marmara Sea segments (Hubert- Ferrari et al., 2000), the expectancy of a large earthquake in the Marmara Sea increased enormously. Estimation of ground motion and seismic hazard in Istanbul was studied using probabilistic methods (Atakan et al., 2002; Erdik et al., 2004; Ansal et al., 2009). Earthquake ground motion estimation can also be represented by the simulation of synthetics through stochastic or hybrid approaches. These approaches were used to perform earthquake scenarios studies (Aagaard et al., 2008; Sorensen et al., 2007).

In this study, we used a stochastic finite-fault simulation technique based on a dynamic corner frequency developed by Motazedian and Atkinson (2005) to simulate strong ground motions due to scenario earthquakes for the city of Istanbul. In this approach, the finite source is represented by a rectangular plane, which is divided into a number of small sub-faults. The rupture starts from the hypocenter and propogates kinematically (Hartzell, 1978) triggering each sub-fault when it reaches its center. Regional an-elastic attenuation, geometric spreading and site effects are included in the model. The total ground motion at an observation point is obtained by summing up the contribution of each sub-fault with an appropriate delay time. This method conserve the total radiated energy at the high frequencies regardless of the sub-fault size and it is applicable to a broader magnitude range.

Development of a reliable synthetic ground motion database for Istanbul by using the finite fault model can be useful for several activities in the profession, such as performance and loss estimates on regional scale or for individual projects, insurance applications and development of new design methodologies.

2. DATA DESCRIPTION

An M_l 5.1 earthquake that occurred on July, 25, 2011 is used as a case study to validate our source, path and site model parameters for the regional stochastic ground motion simulation of the greater Istanbul area. Epicentral coordinates of the earthquake is reported by the Kandilli Observatory and Earthquake Research Institute (KOERI) as 40.82°N – 27.75°E with a focal depth of 15.3 km. The earthquake was associated with the western segments of NAF in the Marmara Sea. The focal mechanisms performed by moment tensor solution indicate that this earthquake had a right lateral strike-slip with the strike and dip angles 75° and 65°, respectively. The earthquake was recorded at twenty strong ground motion stations in and around Istanbul and four ocean-bottom stations, operated by the KOERI, which have epicentral distances ranging from 18 km to 132 km. The simulation of this earthquake is performed using the recordings of 13 stations with the epicentral distances varying between 24km and 95km. The location of the stations used in the simulation and focal mechanism solution are shown in Figure 1. The sampling intervals of the records change as 0.01 and 0.005 sec. All data used in this study were band-pass filtered (0.20–25 Hz) using a fourth order Butterworth filter after baseline correction. Detailed site classification information is available for the recording stations with most of them having an average shear wave velocity of 320 m/sec. Therefore NEHRP-D soil site amplification values are used as proposed by Boore and Joyner (1997). Information on the stations and the processed data are shown in Table 1.

Figure 1. The location of the stations used in the simulation and focal mechanism solution of the M_l 5.1 Marmara Sea earthquake of July 25, 2011

Table 1.Station information and processed data

Station	Code	Latitude (°, N)	Longitude (°, E)	Rjb (km)	PGA (NS, cm/sec^2)	PGA(EW, cm/sec^2)
ZYTAL	R02	40.99	28.91	94.10	3.20	3.70
AVCEM	R05	41.00	28.71	78.25	0.51	2.55
KRTTP	R15	40.98	28.88	91.59	3.06	3.23
GUNGR	R17	41.01	28.88	92.23	3.60	3.08
BAHBL	R30	40.99	28.85	89.69	3.07	4.32
KAKML	R63	40.99	28.79	84.55	2.57	2.48
BAHHI	R65	41.00	28.84	89.02	3.31	3.26
AGPIO	R88	40.97	28.73	79.58	3.78	3.23
AVIIO	R89	40.98	28.71	77.55	3.61	2.28
ZAVKO	R90	40.99	28.92	95.15	5.03	5.47
BOTAS	E5	40.99	27.98	23.82	15.37	10.39
HVHRB	E4	40.96	28.83	87.14	4.20	5.01
SINOB	E1	40.99	28.54	64.65	3.23	2.53

3. SIMULATION METHODOLOGY AND MODELING PARAMETERS

Stochastic finite fault modeling based on a dynamic corner frequency approach is used to generate synthetic records for a specified region by defining the input parameters of the seismic source, wave propagation and site effects. Point source modeling does not include the effects of a large source such as geometry of rupture, slip inhomogeneity and directivity, which have significant effects on the amplitude, frequency content and duration of simulated ground motions. Therefore, stochastic finite-fault models have been developed to simulate large earthquakes (Beresnev and Atkinson, 1997, 1998a, b). In this approach, finite source is represented by a rectangular plane, which is divided into a number of small sub-faults. The rupture starts from the hypocenter and propogates kinematically (Hartzell, 1978) triggering each sub-fault when it reaches its center. Regional an-elastic attenuation, geometric spreading and site effects are included in the model. The total ground motion at an observation point is obtained by summing up the contribution of each sub-fault with an appropriate delay time.

In this study, the simulations have been performed based on the dynamic corner frequency approach using the modified version of the EXSIM software (Boore, 2009). The source parameters of the M_l 5.1 Marmara Sea earthquake covered in Section 2 such as moment magnitude, fault mechanism, depth of the fault and the epicenter location were used as reported by KOERI. Fault length and width were calculated as 3kmx3km. Sub-fault dimensions were chosen as 1kmx1km. A random distribution of slip on the fault plane was assumed in all simulations. In the stochastic method, the attenuation effects of the propagation path are modeled through the empirical *Q* and geometric spreading models. Geometric spreading functions and frequency dependent *Q* used in the simulation were taken from Ansal et al. (2009). Distance dependent duration is defined by the following duration model:

$$T = T_0 + 0.07R \tag{3.1}$$

Where, T_0 is the source duration (equal to the reciprocal of the corner frequency) and R is the hypo-central distance. To account for the site effect, NEHRP-D soil site amplification values are used as proposed by Boore and Joyner (1997). The spectra were also attenuated by the kappa operator, which controls the path-independent high-frequency decay of the spectrum (Anderson and Hough, 1984). Kappa was taken as 0.05, which is a typical value for NEHRP-D type soils. The modeling parameters used for the simulations of the July 25, 2011 Marmara Sea earthquake are listed in Table 2.

Table 2. Finite Fault Model Parameters

Parameters	Parameter Value
Fault orientation (Strike/Dip)	75°/65°
Depth of upper edge of fault (km)	13.5
Fault length and width (km)	3x3
Sub-fault dimensions (km)	1x1
Moment magnitude	4.9
Stress drop (bars)	70
Crustal shear wave velocity (km/sec)	3.8
Crustal density (g/cm^3)	2.8
Rupture velocity (km/sec)	0.7 x(shear wave velocity)
Attenuation, Q(f)	$Q(f)=180f^{0.45}$
Geometric spreading	$1/R$ ($R \leq 30$km) $1/R^{0.4}$ ($30<R<60$km) $1/R^{0.6}$ ($60 \leq R<90$km) $1/R^{0.8}$ ($90 \leq R<100$km) $1/R^{0.5}$ ($R \geq 100$ km)
Duration Model	T_o+0.07R
Kappa	0.05
Windowing-function	Saragoni-Hart
Crustal amplification	-
Site amplification	NEHRP D (Boore and Joyner, 1997)
Pulsing percentage	50
Slip Distribution	Random Slip

3.1. Validation of Finite Fault Model and Simulation Results

We tried different stress drop values and crustal shear wave velocities to observe their effect on ground motion shaking level and frequency amplitudes. For each test model, we compared the waveforms and the Fourier Amplitude Spectra of the synthetic ground motions with real recordings.

The calibration of adopted parameters is done based on the modal bias between the simulations and recordings defined as an error function in the frequency domain as shown in Equation 3.2 (Castro et al., 2008).

$$E(f) = \frac{1}{n}\sum_{i=1}^{n} \log\left(\frac{Ai(f)observed}{Ai(f)synthetic}\right) \tag{3.2}$$

Where, n is the number of stations used in simulations and $Ai(f)$ is the acceleration spectrum of the i^{th} station. This model misfit function is minimized in the frequency range of 0.25–25 Hz.

Figure 2 displays the variation of the modal bias for different stress-drop values and shear wave velocities. Stress drop of 100 bars minimizes the error in the $f < 10Hz$ frequency part, but simulated peak ground acceleration (PGA) values overestimate the observed values. It can be observed that the decreasing the shear wave velocity mostly effects the high frequency part ($f > 10Hz$) and increases the average modal bias.

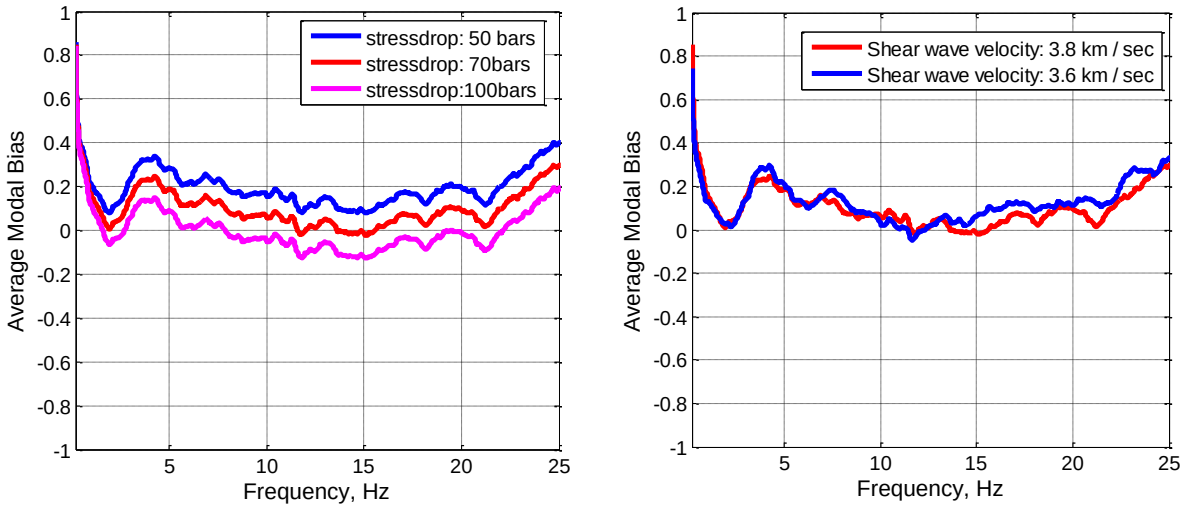

Figure 2. Average modal bias comparison

Using a stress drop of 70 bars and a shear wave velocity of 3.8 km/sec in our model minimizes the overall modal bias. By using the calibrated model parameters, we obtain simulated acceleration time histories and Fourier Amplitude Spectra for all recording stations. In Figure 3, synthetic ground motions are compared with North-South and East-West components of observed ground motions at selected stations. Smoothed Fourier amplitude spectra of simulated and average observed ground motions are also compared in Figure 3. Simulated acceleration time histories in Figure 3 start invariably at 20 sec. This is accommodated by EXSIM to introduce a pre-event pad or to account for pre-arrival tails due to non-causal filters.

A good agreement between the simulated and observed ground motions is obtained both in time and frequency domains. This suggests that calibrated model parameters can be used in the regional ground motion simulation of the Istanbul area for a Mw 7.4 earthquake.

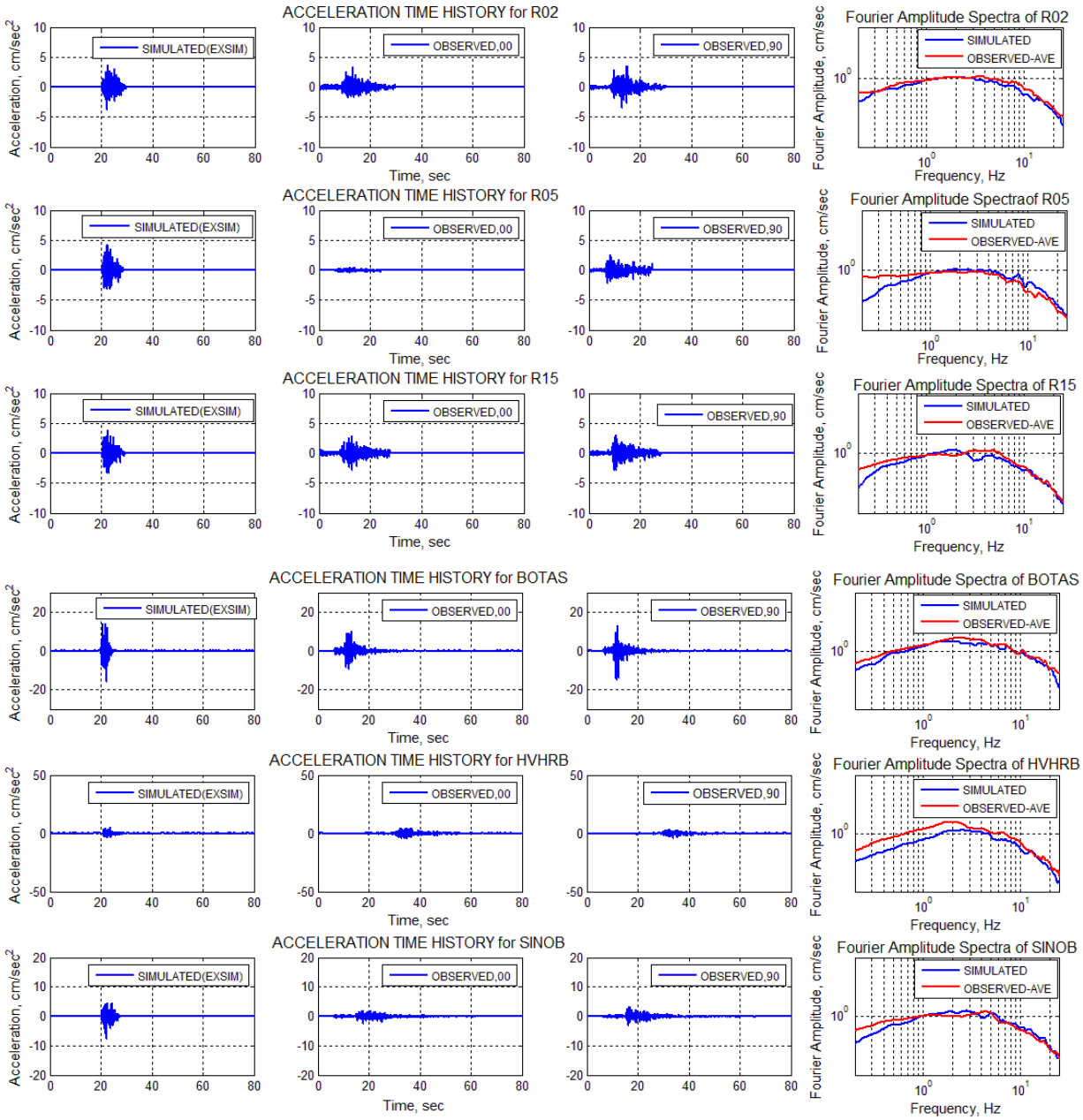

Figure 3. Comparison of time histories and Fourier spectra of synthetics with real data

PGAs and PGVs of station recordings and simulation results are compared with the median±1σ of the Next Generation Attenuation (NGA) Models for NEHRP D soil site conditions, represented with a Vs30=270m/s in Figure 4. We implemented the ground motion prediction equations of Abrahamson and Silva (2008), Boore and Atkinson (2008), Campbell and Bozorgnia (2008), and Chiou and Youngs (2008); these models are abbreviated as AS08, BA08, CB08, and CY08, respectively. We see that the observed and simulated PGAs and PGVs are below the median values estimated by the attenuation models for distances between 20km and 30 km. At large distances, i.e. > 60 km the agreement of PGVs from the simulation and the attenuation models is relatively good.

When we compare the geometric means of the observed accelerations and velocities with their simulated counterparts, we note that the simulated PGAs and PGVs are slightly larger than the recorded ones (i.e with residuals varying between -0.3 and +0.1 for both PGA and PGV). One station, R05, recorded very low accelerations on its NS component (Table 1). We speculate that there may be a problem with the NS component of this station. In Figure 4 the low entry at 80 km is associated with

station R05. The modal bias on the hand varies between ~0 and +0.2 over the frequency range of 1-23 Hz as shown in Figure 2.

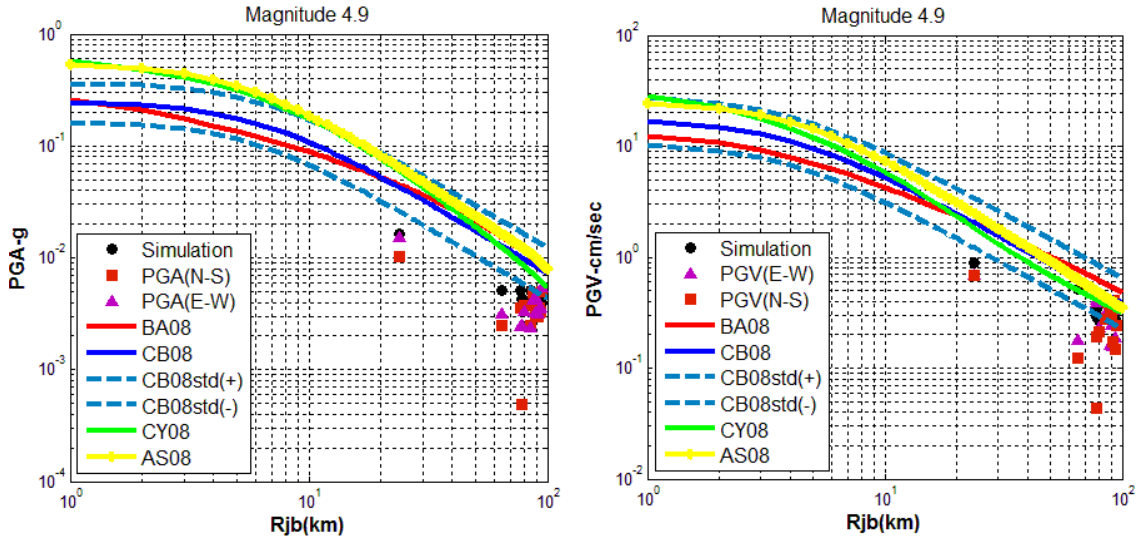

Figure 4. Comparison of simulated and real data with NGA relationships for the M_w 4.9, July 25, 2011 Marmara Sea earthquake

4. SCENARIO EARTHQUAKES AND REGIONAL SIMULATION

For the regional stochastic simulation, the greater Istanbul area is divided into approximately 12,000 grids of size 800m x800m. Synthetic site-specific ground motions are generated for each grid, using fault rupture scenarios, systematically-calibrated model parameters, and detailed site investigation studies. We simulate the expected ground motions from scenario M_w 7.4 events considering the closest segments of the NAF to the city of Istanbul. The scenario earthquakes near Istanbul can involve individual and combined ruptures of the Central Marmara Fault (CMF) and North Boundary Fault (NBF) segments. In this study, we only present rupture scenarios on the CMF segment located about 20–30 km southwest of Istanbul, because they are expected to create the strongest shaking levels in the city.

4.1. Characterization of earthquake scenarios

In order to make a comparison between different scenarios, we have defined three different nucleation points. For the first scenario, the nucleation point is located at the westernmost edge of the fault and ruptures unilaterally towards east. Other nucleation points are defined in the center of the fault (Scenario 2-bilateral rupture) and at the left end of the fault (Scenario 3-unilateral rupture towards west). Three nucleation points are located at a hypo-central depth of 12km. A random slip model is used in all simulations. The location of the nucleation points and scenarios are shown in Figure 5.

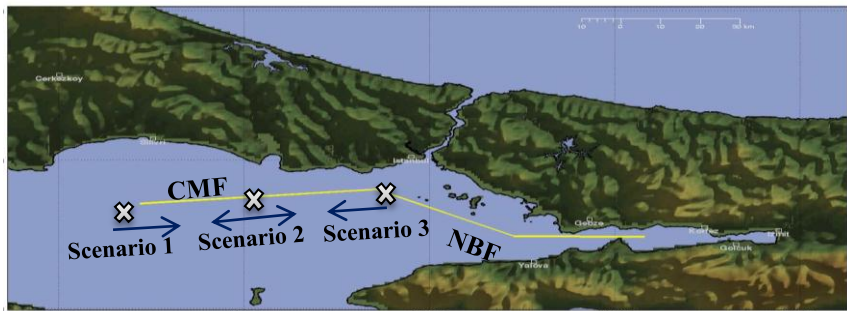

Figure 5. Three rupture scenarios defined based on the location of the nucleation points

A total fault length of 100 km is used. The fault width is assumed as 20 km based on the depth distribution of local seismicity (Gurbuz et al., 2000). Adopted source parameters of the scenario earthquake are listed in Table 3.

Table 3. Source parameters of the scenario earthquake

Parameters	Parameter Value
West end coordinate (CMF)	40.80N-27.68E
East end coordinate (CMF)	40.89N-28.87E
Fault orientation (Strike/Dip)	83°/90°
Depth of upper edge of fault (km)	2.0
Fault length and width (km)	100x20
Subfault dimensions (km)	5x5
Moment magnitude	7.4
Stress drop (bars)	100
Crustal shear wave velocity (km/sec)	3.8
Crustal density (g/cm^3)	2.8
Rupture velocity (km/sec)	0.7 x(shear wave velocity)

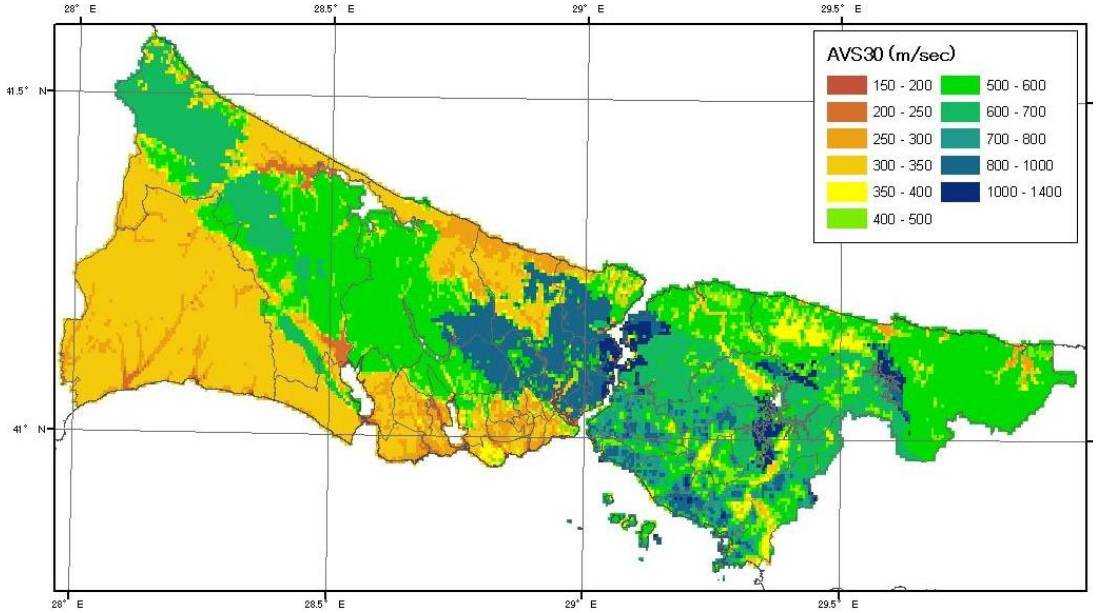

Figure 6. Vs30 Soil Classification Map of Istanbul (IBB-OYO- KOERI, 2009)

4.2. Ground motion simulation results

The effect of different nucleation points, as well as that of different stress drop values and pulsing percentage is tested by calculating the PGA's and PGV's of each scenario. Simulation results show that the location of the nucleation point has a significant effect on the distribution of the ground motion. PGA and PGV distribution of each scenario are shown in Figure 7.

Directivity effect is clearly seen in the Scenario 1, where the PGA and PGV values are increased in the forward directivity and decreased in the backward directivity directions. It is observed that the peak ground accelerations with a magnitude of up to 600cm/sec^2 and peak ground velocities of up to 60cm/sec are predicted in the southern part of the city, which are at the closest region to fault plane. In our study, Scenario 2 can be assumed as a worst-case scenario where the highest shaking level is estimated at the southernmost part of the Istanbul. In Scenario 3, the rupture is extended toward the west and the shaking level is increased in a narrower region at forward stations. The backward stations are not affected significantly in terms of PGA and PGV levels as compare to other scenarios.

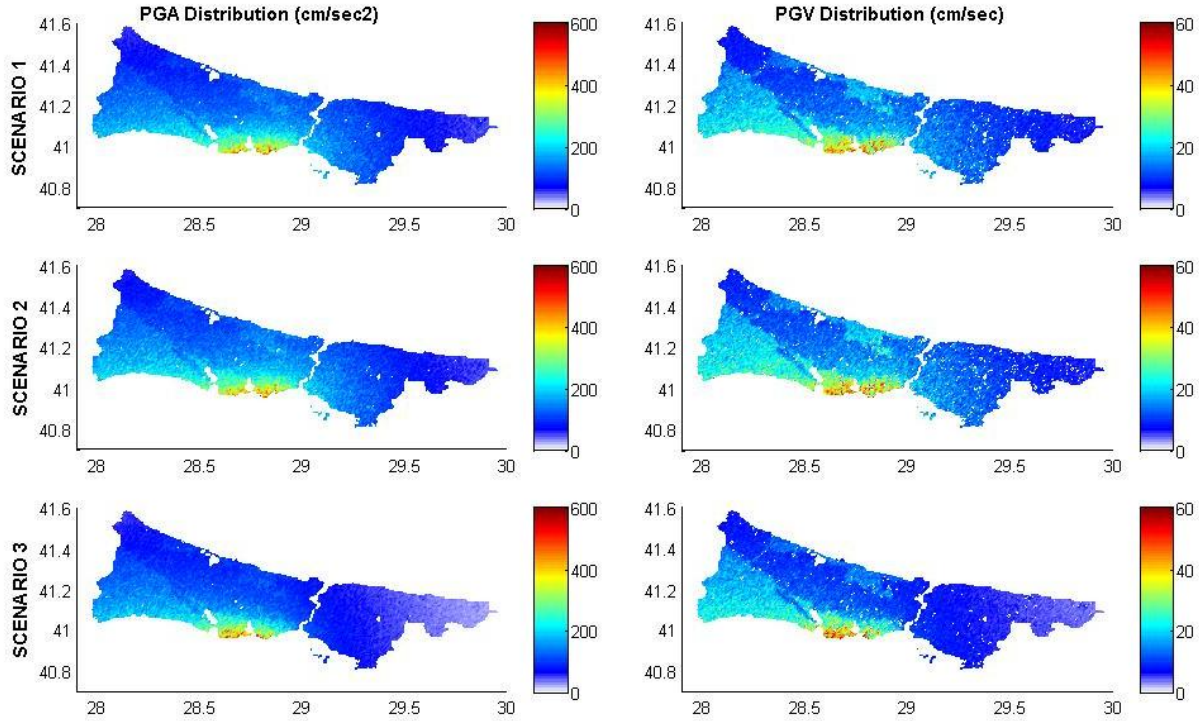

Figure 7. PGA and PGV distribution in Istanbul for different scenarios

The effect of stress drop on ground motion distribution is tested by increasing it from 100 to 130 bars in each scenario. PGA and PGV differences are calculated for each individual scenario to see the level of changes in the entire region. Since the stress drop parameter affects the high frequency part of simulation, the PGA levels are significantly affected. Increasing the level of stress drop increases the level of PGA by 15-20% as shown in Figure 8. A similar effect is observed for the PGVs, where the level of change is up to 20%. The site amplification effect is clearly seen in the PGA and PGV distribution figure, which is consistent with the Vs30 Soil Classification Map of Istanbul.

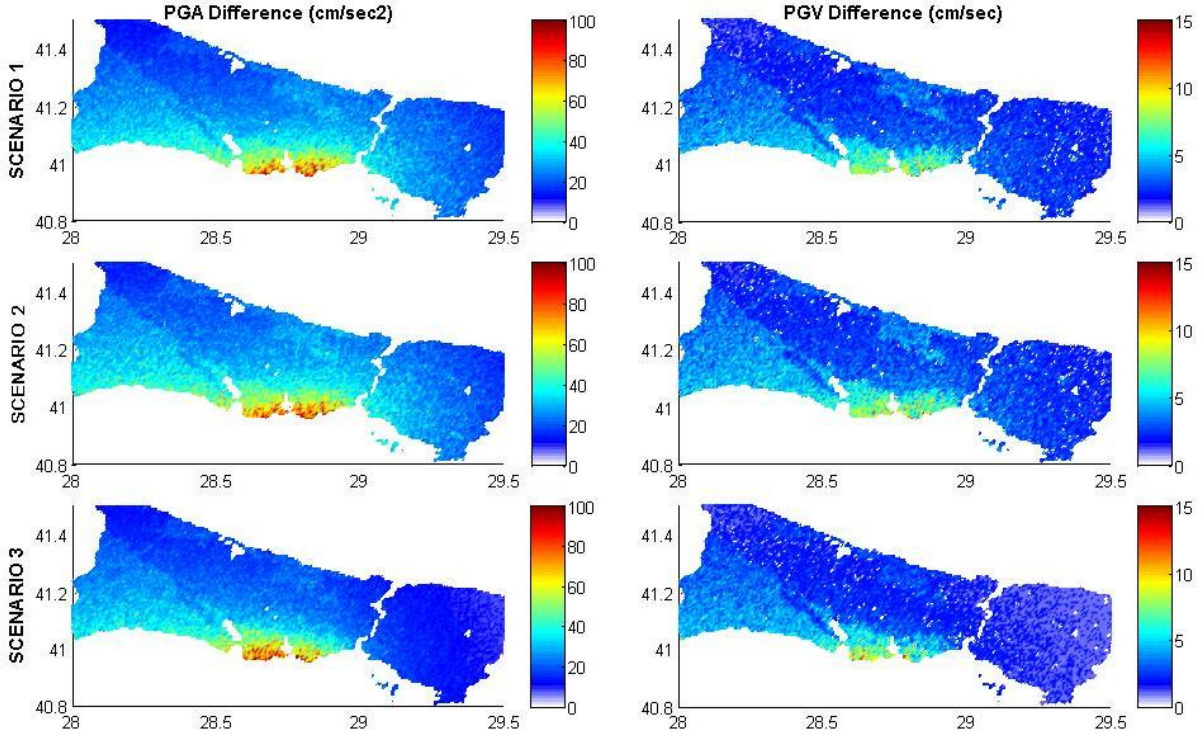

Figure 8. Effect of stress drop change on the distribution of ground motion

We also investigated the effect of the pulsing percentage on the peak ground acceleration and peak ground velocity levels. We decreased the pulsing percentage of 50 to 30 and observed that it results a minor increase on PGA and PGV values. Pulsing percentage mainly controls the low frequencies in spectra, and it can be used to adjust amplitudes of low-frequency motion in finite-fault modeling.

4.3. Comparison of simulation results with NGA relationships

In order to verify the applicability of the scenario results, we compare the synthetic PGA's and PGV's from Scenario 1 with the median±1σ values estimated by NGA models for soil site conditions with Vs30=270m/s (NEHRP D) in Figure 9. In our simulation model, we assigned NEHRP C or D site amplification values to each grid based on their Vs30. Therefore, small discrepancy can occur between synthetics and ground motion prediction equations. Synthetic PGA's are slightly above the median for distances between 10 and 15km, but the PGV's are in good agreement with the median values. Overall, a very good agreement between the NGA models and synthetics are achieved.

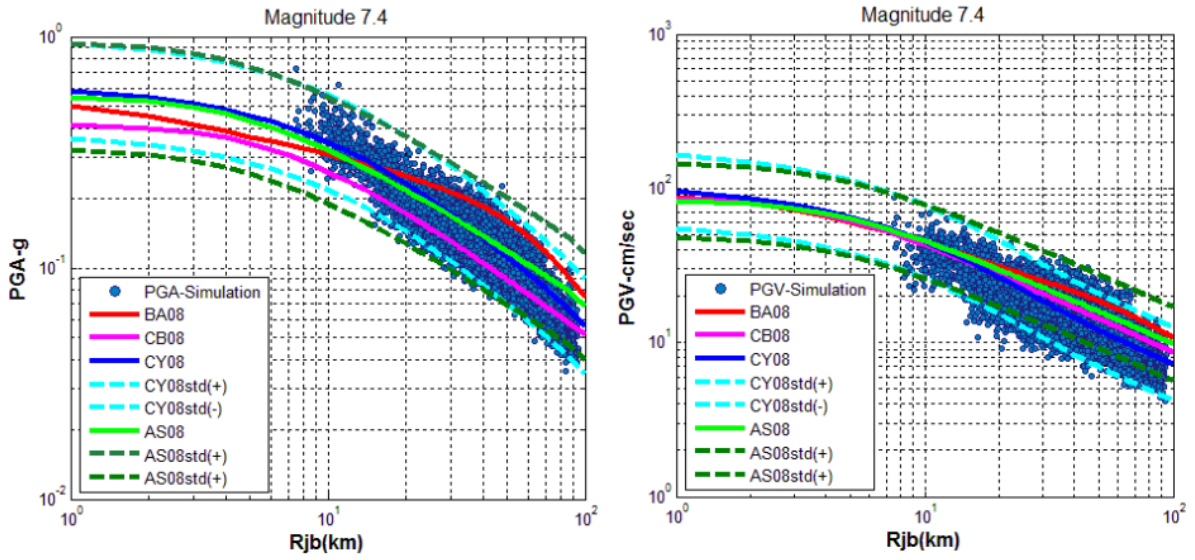

Figure 9. Comparison of synthetic data with NGA models

5. CONCLUSION

In this study, a stochastic finite-fault technique proposed by Motazedian and Atkinson (2005) was used to simulate scenario-based earthquakes (Mw 7.4) for the Istanbul area. The region-specific source, path and site model parameters were calibrated by simulating the Marmara Sea earthquake (M_l=5.1), which occurred on July 25, 2011 and was associated with the North Anatolian Fault. A good agreement between the simulated and observed ground motions was obtained both in the time and frequency domains. Validated model parameters were used in the regional simulation of the Istanbul area. We estimated grid based ground motions in the Istanbul region from scenario earthquakes involving the rupture of the CMF segment of NAF. The effect of different hypocenter locations, stress drop and pulsing area changes on the ground motion level was studied. Simulation results show that the location of the nucleation point has a significant effect on the distribution of the ground motion. Directivity effect was observed in the Scenario 1, where the PGA and PGV values were increased in the forward directivity and decreased in the backward directivity directions. The peak ground accelerations with a magnitude of up to 600cm/sec^2 and peak ground velocities of up to 60cm/sec were estimated in the southern part of the city. It is found that changing the stress drop parameter significantly affects the PGA and PGV levels, but change in the level of pulsing percentage area had no effect on these values. Simulations were compared with the NGA models to find a good match between them.

Our future studies will focus on using different rupture scenarios including individual ruptures of the NBF and the combined ruptures of CMF and NBF. We will also perform sensitivity analyses to investigate the effects of important parameters such as stress drop, rupture velocity and pulsing percentage on ground motion. Our aim is to develop a reliable synthetic ground motion database for Istanbul over a dense grid.

REFERENCES

Aagaard, B.T., Brocher, T.M, Dolenc, D., Dreger, D., Graves, R.W., Harmsen, S., Hartzell, S., Larsen, S., McCandless, K., Nilsson, S., PeterssoN, N.A., Rodgers, A., Sjögreen, B., and Zoback, M.L. (2008). Ground-motion modeling of the 1906 San Francisco earthquake, Part II: Ground-motion estimates for the 1906 earthquake and scenario events, *Bull. Seismol. Soc. Am*., **98**, 1012–1046.

Anderson, J. G. and Hough, S.E. (1984). A model for the shape of the Fourier spectrum of acceleration at high frequencies, *Bull. Seism. Soc. Am*., **74**, 1969–1993.

Ansal, A., Akinci, A., Cultrera, G., Erdik, M., Pessina, V., Tonuk, G., and Ameri, G. (2009). Loss estimation in Istanbul based on deterministic earthquake scenarios of the Marmara Sea region, *Soil Dynamics and Earthquake Engineering*, **29**, 699–709.

Atakan, K., Anibal, O., Meghraoui, M., Barka, A.A., Erdik, M., and Bodare, A. (2002). Seismic hazard in Istanbul following the 17 August 1999 Izmit and 12 November 1999 Duzce earthquakes. *Bull. Seismol. Soc. Am*., **92**, 466– 482.

Beresnev, I., and Atkinson, G.M. (1997). Modeling finite-fault radiation from the ωn spectrum, *Bull. Seismol. Soc. Am*., **87**, 67–84.

Beresnev, I., and Atkinson, G.M. (1998a). FINSIM—a FORTRAN program for simulating stochastic acceleration time histories from finite faults, *Seism. Res. Lett.* **69**, 27–32.

Beresnev, I., and Atkinson, G.M. (1998b). Stochastic finite-fault modeling of ground motions from the 1994 Northridge, California, earthquake. I. Validation on rock sites, *Bull. Seismol. Soc. Am*., **88**, 1392–1401.

Boore, D.M., and Joyner, W. (1997). Site amplification for generic rock sites, *Bull. Seism. Soc. Am*., **87**, 327–341.

Boore, D.M. (2009). Comparing Stochastic Point-Source and Finite-Source Ground-Motion Simulations: SMSIM and EXSIM, *Bull. Seism. Soc. Am.,* Vol. **99**, No. 6, 3202–3216.

Castro, R. R., Pacor, F., Franceschina, G., Bindi, D., Zonno, G., and Luzi, L. (2008). Stochastic strong motion simulation of the Mw 6 Umbria– Marche earthquake of September 1997: Comparison of different approaches, *Bull. Seismol. Soc. Am.* **98**, 662–67.

Erdik, M., Demircioglu, M., Sesetyan, K., Durukal, E., and Siyahi, B. (2004). Earthquake hazard in Marmara region, Turkey. *Soil Dyn Earthquake Eng;* **24**:605–31.

Gurbuz, C., Aktar, M., Eyidogan, H., Cisternas, A., Haessler, H., Barka, A., Ergin, M., Turkelli, N., Polat, O., Ucer, S.B., Kuleli, S., Baris, S., Kaypak, B., Bekler, T., Zor E., Bicmen, F., and Yoruk, A. (2000). The seismotectonics of the Marmara region (Turkey): results from a microseismic experiment, *Tectonophysics* **316**, 1–17.0.

Hartzell, S. (1978). Earthquake aftershocks as Green's functions, *Geophys. Res. Lett*. **5**, 1–14.

Hubert-Ferrari, A., Barka, A., Jacques, E., Nalbant, S.S., Meyer B., R. Armijo, P. Tapponnier, and G.C.P. King (2000). Seismic hazard in the Marmara Sea region following the 17 August 1999 Izmit earthquake, *Nature* **404**, 269–273.

IBB-OYO-KOERI. (2009). İstanbul'un Olası Deprem Kayıpları Tahminlerinin Güncellenmesi İşi, *Proje Çalışma Raporu*, Boğaziçi Üniversitesi, Deprem Mühendisliği Bölümü, İstanbul.

Motazedian, D., and Atkinson G. M. (2005). Stochastic finite-fault modeling based on a dynamic corner frequency, *Bull. Seismol. Soc. Am*. **95**, 995–1010.

Sørensen, M., Pulido, N., Atakan, K. (2007). Sensitivity of Ground-Motion Simulations to Earthquake Source Parameters: A Case Study for Istanbul, Turkey, *Bull. Seismol. Soc. Am*, Vol. **97**, No. **3**, p. 881–900.